1

DENSITY, THERMAL PROPERTIES, AND THE GLASS TRANSITION TEMPERATURE OF GLASSES

Steve Feller

Physics Department, Coe College, Cedar Rapids, IA, USA

Part I: Introduction to Physical Properties and Their Uses

Any computer-generated or spectroscopic determination of the atomic structure of glass is tempered by the necessity that the resulting structural model be consonant with physical property measurements. As a result the basic physical properties play a key role in the acceptance of any model of atomic arrangements. In this chapter, two of the most fundamental properties are examined: density (ρ) and thermal properties with a focus on the glass transition temperature (T_g). How these measurements are made and interpreted will be discussed. Also, some comparisons between the resulting properties and models of glass structure are given.

First, however, a note of caution is provided. It is not possible to go from direct measurements of the physical properties to a unique model of atomic arrangement. This multiplicity of paths is an example of an *ill-posed problem*. What can be done is to use experimental property data to provide a consistency check on models. That is significant.

Density is perhaps the single-most fundamental and important measure of a glass. Its value is needed in manifold experimental techniques such as neutron, electron, and

Modern Glass Characterization, First Edition. Edited by Mario Affatigato.

x-ray scattering. It is also an essential value in molecular dynamics simulations. In addition, density stands on its own as an intrinsic property capable of casting light on various ranges of order within glasses [1].

Furthermore, density can be used to extract a variety of useful volumes including the molar volume, the volume per mole glass former, and for a given model of atomic structure, the volumes of the individual atomic-level structural units themselves. Another useful parameter directly derived from density is the dimensionless packing fraction, the ratio of filled space to total volume within a glass [2]. Additionally, as these property data have become available from a wide variety of glass systems over extended compositional regimes, it has become possible to gain greater insight into atomic arrangement comparisons between systems. What has emerged from this work is a comprehensive set of data which has been quantitatively linked to models of both the short range and intermediate order.

The glass transition temperature is a defining universal condition for a material to be a glass. It is an independent and useful parameter in its own right but the experimental thermogram can also be used to determine other temperatures as well (recrystallization temperature, melting points, pre-glass transition temperature exothermic rearrangements, and more) and to extract the fictive temperature. It will be shown in this chapter that the atomic structure of glass gives rise to systematic changes in T_g with composition. For example, it will be shown that in borate glasses the presence of tetrahedral borons increases $T_{g.}$

Part II: Density

1.1 DENSITY: EXPERIMENTAL BACKGROUND AND THEORY

1.1.1 Overview

In this section, methods of how density is determined in a number of ways will be discussed at some length. Density, ρ, is defined by

$$\rho = \text{mass}/\text{volume}. \tag{1.1}$$

Density is a function of a number of experimental variables including ambient temperature, chemical purity of the sample, the presence of bubbles, thermal history (fictive temperature), and more. Thus, the conditions under which the samples were prepared and the density measured need to be specified in any reporting of such experimental data. In the following it is assumed that a sample of high quality has been prepared without bubbles, with a known thermal history, and whose composition is well characterized.

In summary, in this section of this chapter several of the various methods by which density is determined are described. Later in the chapter some illustrative examples of density trends in glass forming systems are examined.

1.1.2 Experimental Methods and Theory

1.1.2.1 Direct Determination of Mass and Volume In principle, the most straightforward way of determining density is the direct determination of the mass and volume of the object. For example, a high quality cylinder may have its volume determined by measuring its diameter D, and length L, and using a precision mass scale for mass M. Then the density would be simply

$$\rho = M/V = M/(\pi D^2 L/4) = (4M/(\pi D^2 L) \tag{1.2}$$

This method is not often used for glasses due to the need for such highly symmetric shapes. The most important source of error in this method will likely be in the determination of volume since mass may be routinely determined to high accuracy in a modern laboratory.

1.1.2.2 Archimedes' Principle: Wet/Dry Weighing This beautiful method relies on weighing the glass sample in both a liquid ($W_{\text{sample in liquid}}$) and in air ($W_{\text{sample in air}}$). Separate measurements of mass and volume are not needed. Rather, Archimedes' principle states that the buoyant force, B, exerted on a solid immersed in a liquid is given by the weight of the displaced fluid, $W_{\text{displaced fluid}}$:

$$B = W_{\text{displaced fluid}} = \rho_{\text{liquid}} V_{\text{sample}} g \tag{1.3}$$

where ρ_{liquid} is the density of the liquid, V_{sample} is the sample volume, and g is the acceleration due to gravity. Ignoring the small buoyant force of air makes, $W_{\text{sample in air}} = W_{\text{sample}}$, and allows $W_{\text{sample in liquid}}$ to be expressed by

$$W_{\text{sample in liquid}} = W_{\text{sample in air}} - \mathrm{B} \tag{1.4}$$

Noting that V_{sample} is $M_{\text{sample}}/\rho_{\text{sample}}$ produces

$$\begin{aligned} W_{\text{sample in liquid}} = W_{\text{sample in air}} - B &= W_{\text{sample in air}} - \rho_{\text{liquid}} V_{\text{sample}} g \\ W_{\text{sample in liquid}} &= W_{\text{sample in air}} - \rho_{\text{liquid}} \, (M_{\text{sample}}/\rho_{\text{sample}}) g \\ W_{\text{sample in liquid}} &= W_{\text{sample in air}} - \rho_{\text{liquid}} \, (W_{\text{sample}}/\rho_{\text{sample}}) \end{aligned} \tag{1.5}$$

This leads to the working equation

$$\rho_{\text{sample}} = \rho_{\text{liquid}} (W_{\text{sample in air}}/(W_{\text{sample in air}} - W_{\text{sample in liquid}})) \tag{1.6}$$

The density is then determined using Eq. 1.6 after having measured $W_{\text{sample in liquid}}$ and $W_{\text{sample in air,}}$ and with knowledge of ρ_{liquid}. This method is commonly used and has several advantages.

- There is no limitation on the density of the sample.
- It is inexpensive to perform.

- Sample shape does not matter.
- Pure water can often be used as the working fluid if the density is not very high and if the sample is not hygroscopic.

There are some disadvantages that make it difficult to exceed 1% accuracy in the final density.

- The density of the working fluid tends to be more temperature dependent than the sample leading to the need for good temperature control of the fluid.
- It is not easy to perform the wet weighing and one must be extremely careful for precision results. Be on the lookout for fluid adhering to the fine thread that holds the sample.
- Bubbles would lead to an underreporting of the density.

1.1.2.3 Archimedes' Principle: Sink-Float Method The *sink-float* method also relies on Archimedes' Principle [1]. In this technique, the sample is initially sunk in a solution of two miscible fluids such as acetone ($\rho_{\mathrm{ace}} = 0.78$ g/cc) and diiodomethane ($\rho_{\mathrm{dii}} = 3.32$ g/cc). The acetone-diiodomethane solution that is prepared is chosen to have a slightly smaller density than that approximated for the sample. Drops of diiodomethane are added until the sample floats (usually done in duplicate to ensure reliability and to provide a better estimate of error). A magnetic stirrer stirs the solution to ensure homogeneity.

It has been determined experimentally that this additive solution is fully miscible for these fluids. Thus, the volumes of the two fluids very nearly satisfy

$$V_{\mathrm{liquid}} = V_{\mathrm{ace}} + V_{\mathrm{dii}} \tag{1.7}$$

Under these conditions, at the point where the sample just floats

$$\begin{aligned}\rho_{\mathrm{sample}} &= \rho_{\mathrm{liquid}} = M_{\mathrm{liquid}}/V_{\mathrm{liquid}} = (M_{\mathrm{ace}} + M_{\mathrm{dii}})/(V_{\mathrm{ace}} + V_{\mathrm{dii}})\\ &= (1 + M_{\mathrm{dii}}/M_{\mathrm{ace}})/((V_{\mathrm{ace}} + V_{\mathrm{dii}})/M_{\mathrm{ace}})\end{aligned}$$

or

$$\rho_{\mathrm{sample}} = \rho_{\mathrm{ace}}(1 + \mathrm{Q})/((1 + \mathrm{Q})\ \rho_{\mathrm{ace}}/\rho_{\mathrm{dii}}) \tag{1.8}$$

where Q is the mass ratio, $M_{\mathrm{dii}}/M_{\mathrm{ace}}$.

Equation 1.8 is the working equation for density for the sink-float method. Note that in the limit of Q going to zero, the density becomes that of acetone whereas as Q becomes large the equation predicts a density near that of diiodomethane. The range of observed glass densities is therefore, 0.78 g/cc $< \rho_{\mathrm{glass}} <$ 3.32 g/cc.

If the densities of the two fluids are well known then the sink-float method has the advantage of needing just the masses of the two fluids (easy to measure) to determine the density of a glass flake as small as a few tens of milligrams. Furthermore, the sample may be of an irregular shape. The method has the disadvantage of being limited to the range of the densities of the working fluids, as mentioned above.

In some cases the fluids may react with the samples. In such circumstances the sample density may be found by bracketing the glass densities with mixtures of closely varying densities.

1.1.2.4 Pycnometry Gas pycnometry is an experimental method that determines volume. It involves the use of the ideal gas law to convert pressure changes to volume determination.

In the following discussion, we assume the use of helium, the least reactive, most penetrating, and most ideal of all gases, although other gases may be used such as nitrogen. Two volumes, the reference volume and the sample volume are used as shown below in Figure 1.1.

Previous to using the device it is assumed that the reference and sample chamber volumes have been calibrated. Standard metal spheres are typically used for this step. The reference and sample volumes are denoted V_1 and V_2 as shown in Figure 1.1.

A sample of unknown volume, V_s, is inserted into the sample chamber (in the photograph of the instrument in Figure 1.2, this is done by opening the black screw top lid and inserting the sample in a sample cup). Initially V_1 is filled with He when valve 1 is opened and valve 2 is left closed. Pressure P_1 is measured. Valve 2 is opened and Pressure P_2 is observed. For fixed temperature and cancelling out a common atmospheric pressure term the ideal gas law becomes

$$P_1 V_1 = P_2(V_1 + V_2 - V_s) \tag{1.9}$$

This equation can be rearranged to find the working equation for V_s.

$$V_s = V_1(1 - P_1/P_2) + V_2 \tag{1.10}$$

Use of a high quality electronic balance to find the sample mass then completes the measurement for density.

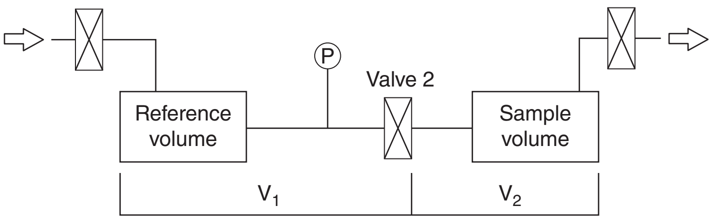

Figure 1.1. Schematic of a pycnometer's operation.

Figure 1.2. A Quantachrome® manual pycnometer.

This method has several advantages.

- There is no bound on what the density of the sample is.
- After the initial purchase of the pycnometer and balance (both may sum to $10,000 or more in 2015 dollars) it is inexpensive to perform measurements. A tank of helium may last years.
- Shape does not matter. Powders can be measured readily.
- It is easy to perform multiple volume determinations on the same sample and determine high precision statistical measures of accuracy.

There are some disadvantages as well.

- There is a fairly strong temperature dependence on the pressure leading to the need for good temperature control of the instrument.
- Outgassing of the sample can be an issue.
- Be wary of bubbles. The presence of bubbles will give an artificially low density result.
- Sample size is limited by the sample cell. Typically, it is difficult to measure accurately sample volumes below 0.5 cc or so.

1.1.2.5 The Gradient Density Column—the ASTM D1505 Method for Determining Density In this method a long tube is filled with a fluid whose density changes with height. If the temperature is controlled, this method may be accurate to within 0.05 %. Where accuracy of 0.05 % or better is desired, the gradient tube is made so that vertical distances of 1 mm represent density differences no greater than 0.0001 g/cm^3. The sensitivity of the column is then 0.0001 g/cm^3·mm. For further details, including instrumentation needed, the reader is referred to the American Society for Testing and Materials (ASTM) method which is found at http://www.astm.org/Standards/D1505.htm. Furthermore, there are additional ASTM methods for determining density such as *ASTM D792-08 Standard Test Methods for Density and Specific Gravity (Relative Density) of Plastics by Displacement.*

1.1.3 Instrumentation Used for Determining Density

1.1.3.1 Direct Determination of Mass and Volume *Instrumentation Needed*: Digital micrometer, typically accurate to ±0.00001m or better, and a precision digital balance. A modern digital balance needs to be precise to ±0.0001 g. This would result in density being determined to better than ±0.1%. For example, Masao Kodama found [3] the density of well-characterized boron oxide glass from this method to be 1.839 ±0.001 g/cm^3.

1.1.3.2 Archimedes' Principle: Wet/Dry Weighing *Instrumentation Needed*: Precision digital balance designed to do both dry and wet massings, a suitable and high purity fluid such as mineral oil, distilled water, or reagent grade diiodomethane, a beaker to hold the fluid, and a small container with fine thread to hold the sample for weighing. It is difficult to determine density by this technique to better than 1%. To do better precise temperature control of the fluid and knowledge of the fluid density would be essential. The greater the fluid density, the greater will be the difference in the weighings and hence the more precise the density measurement.

1.1.3.3 Archimedes' Principle: Sink-Float Method *Instrumentation Needed*: Glass cylinder, perhaps 20 cc in capacity or less with a ground glass stopper; suitable, miscible fluids such as reagent grade acetone and diiodomethane; magnetic stirrers with an external stirring apparatus, a microburrette to dispense the denser fluid, and a quality balance. The density maybe readily found to an accuracy of 1%. Relative densities may be found to be better than 0.1%.

1.1.3.4 Pycnometry *Instrumentation Needed*: a pycnometer, a mass balance, a tank of gas, preferably helium, although nitrogen may be used as well. With temperature control or correction density may be found to 0.1% for a sample volume of 1 cc.

1.1.3.5 General Considerations There are several common considerations that make density difficult to determine absolutely. The sample preparation is one such limitation. For example, once again considering boron oxide, there is a variation in density of a few percent in going from a rapidly quenched sample to a well annealed glass [4]. It is best to study samples with similar thermal histories. Relaxation may play a role as the density may slightly vary over time as the sample relieves stress. Also, some techniques exhibit a sample size consideration in terms of precision. This is true for pycnometry and the Archimedes' wet/dry dual weighing methods.

1.1.4 Analysis of Data, Extraction of Useful Information, and Other Ways to Express Density

While density is useful in its own right there are several different ways to present these data in useful forms. Three alternatives will be discussed including molar volume, volume per mole glass former, and packing fraction. This will be followed by a brief discussion of the extraction of atomic level volumes directly from the density.

1.1.4.1 Molar Volume The molar volume, V_{M}, is defined by

$$V_{\mathrm{M}} = \text{Mass of a mole of glass}/\rho \tag{1.11}$$

For a borate glass of composition $\mathrm{RM_2O.B_2O_3}$ the molar volume can be rewritten by

$$V_{\mathrm{M}} = \mathrm{Mass(RM_2O.B_2O_3)}/((1+\mathrm{R})\rho) \tag{1.12}$$

where the factor 1+R comes about because there are R moles of $\mathrm{M_2O}$ and one mole of $\mathrm{B_2O_3}$.

Molar volume may also be written in terms of molar fractions by

$$V_{\mathrm{M}} = \mathrm{Mass(XM_2O.(1-X)B_2O_3)}/\rho \tag{1.13}$$

where X is the molar fraction of alkali oxide and 1−X is the molar fraction of $\mathrm{B_2O_3}$. The units of V_{M} are $\mathrm{cm^3/mol}$ for densities expressed in $\mathrm{g/cm^3}$ and mass in g/mol. The practical benefit of molar volume is the elimination of mass from the density making structural comparisons easier to observe.

As an example, Figure 1.3 shows the molar volumes of the alkali and alkaline-earth borate glass systems as a function of R [5].

Note, for example, in Figure 1.3, that the same trend is observed for molar volumes in the lithium, sodium, magnesium, and calcium borate glasses systems. This presumably implies that in borate systems in which the modifying ion is smaller than oxygen, the molar volume trend is dominated by the boron oxide network.

1.1.4.2 Volume per Mole Glass Former The volume per mole glass former, $\mathrm{V_{mole\ former}}$, is defined by

$$V_{\text{mole former}} = \text{Mass of a mol of glass former}/\rho \tag{1.14}$$

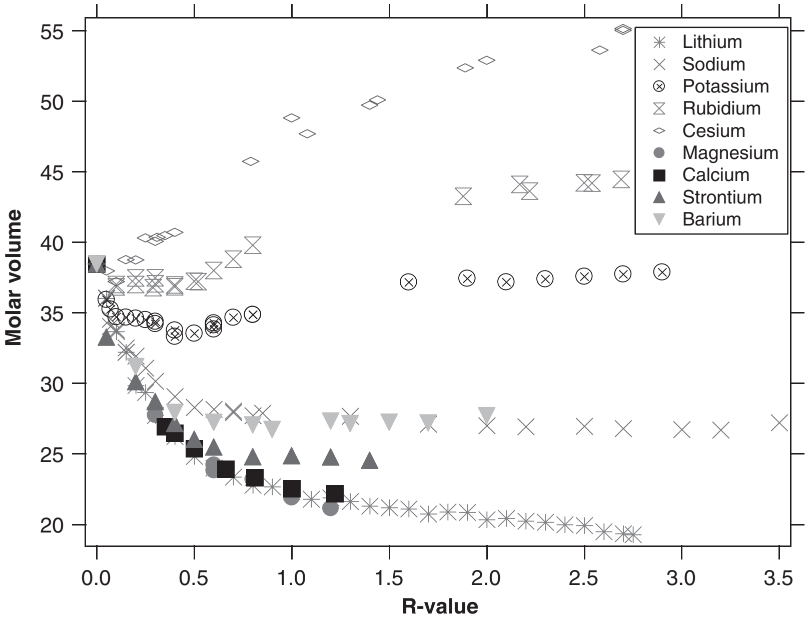

Figure 1.3. Molar volumes of the alkali and alkaline-earth borate glass system [5]. R is the molar ratio of metal oxide to boron oxide. The error is smaller than the symbols used.

For the alkali borate system the volume per mol boron oxide is

$$V_{\text{mole former}} = \text{Mass}(\text{RM}_2\text{O.B}_2\text{O}_3)/\rho \tag{1.15}$$

This may linearize the volume trend (see discussion below of lithium silicates).

A comparison of the volume per mole of glass former three binary glass systems is shown in Figure 1.4 [6]. There is clear evidence in the figure for coordination changes in the borates (3 to 4) and germanates (4 to 5 or 6) by the presence of the minima in the volume per mole of glass former as a function of modifier content. No minimum is seen for the silicates, see Figure 1.4.

1.1.4.3 Packing Fraction The packing fraction, pf, is a dimensionless measure of density and is determined by the ratio of the filled space in a glass to the total volume available

$$\text{pf} = \text{Volume of all ions in a mole of glass}/V_\text{M} = \sum \text{N}_\text{A}(4/3)\,\pi r_i^3/\,V_\text{M} \tag{1.16}$$

Here r_i is the ionic radius of the i^{th} atom in the chemical formula for the glass and N_A is Avogadro's number. Ionic radii are typically determined by diffraction and Shannon provides a good source for such numerical information [7]; see Table 1.1.

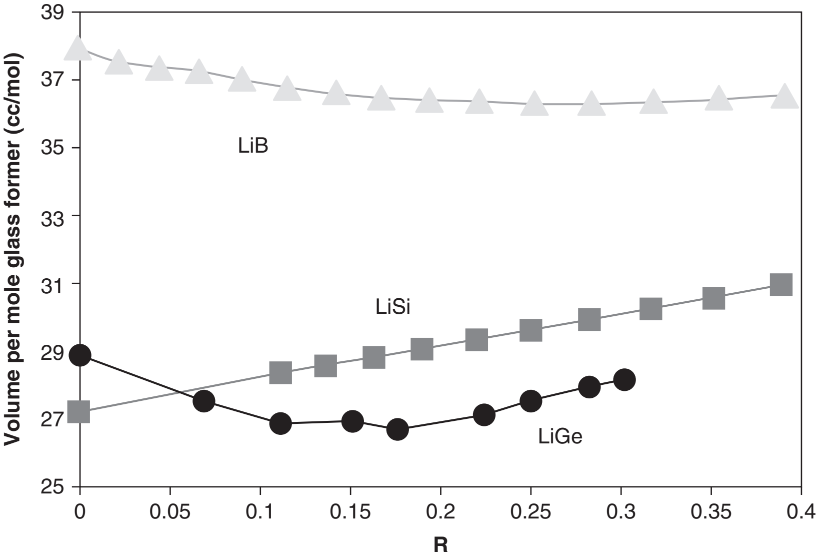

Figure 1.4. Molar volumes per mole glass former in the lithium borate, lithium silicate, and lithium germanate glass systems [6]. R is the molar ratio of lithia to silica, germania, or bora.

Figure 1.5 depicts the packing fractions of the alkali and alkaline-earth borates [8]. The packing trends reveal much about the structure. The lithium and magnesium systems have very similar pf values presumably because these ions are much smaller than oxygen. The result is a common compositional trend for the filling of space by the borate network as the glass is modified.

1.1.4.4 Atomic Volumes from the Alkali and Alkaline-Earth Borate Glass Systems Figure 1.6 depicts the density of the alkali and alkaline-earth borates as function of R, the molar ratio of modifying oxide to boron oxide [5]. It is evident that all systems follow a rapid increase in density followed by either a decrease or a milder increase in the density. Further analysis of the density itself is possible through knowledge of the atomic arrangements. For example, it is possible to determine the volumes of the short-range structural groups through knowledge of the density and the nuclear magnetic resonance (NMR)-determined fractions of the short-range units by

$$\rho(\mathrm{R}) = \text{Mass of the glass structural groups}/\left(\sum (f_i V_i)\right) \tag{1.17}$$

where f_i and V_i are the fractions and volumes of the i^{th} structural group. These structural volumes of the atomic-level units, relative to that of the three-coordinated borons in boron oxide glass are given for the alkali borates in Table 1.2. The structural units in this table are reported as Q^{ni} where the integer n refers to the boron coordination and i denotes the number of bridging oxygens per boron.

TABLE 1.1. Ion coordination and size [7, 8].

	Be	Mg	Ca	Sr	Ba	Li	Na	K	Rb	Cs	O	Si	^{III}B	^{IV}B	^{IV}Ge	^{VI}Ge	P
Coordination	4	6	7–8	8	9	4	6	8	9	10	2	4	3	4	4	6	4
Radius (Å)	0.41	0.86	1.23	1.4	1.61	0.73	1.16	1.65	1.77	1.95	1.21	0.4	0.15	0.25	0.53	0.67	0.31
Radial uncertainty (Å)	0.1	0.06	0.05	0.05	0.05	0.05	0.03	0.02	0.02	0.02	0.01	0.01	0.01	0.01	0.01	0.01	0.01
Volume (Å^3)	0.29	1.50	7.80	11.49	17.48	1.63	6.54	14.71	19.16	31.06	7.42	0.25	0.01	0.07	0.62	1.26	0.12
Volume uncertainty(Å^3)	0.22	0.56	0.95	1.23	1.63	0.34	0.51	0.6	0.8	1	0.37	0.02	0.003	0.008	0.04	0.06	0.02
Fractional volume uncertainty	0.76	0.37	0.12	0.107	0.09	0.21	0.08	0.04	0.04	0.03	0.05	0.08	0.3	0.11	0.06	0.05	0.17

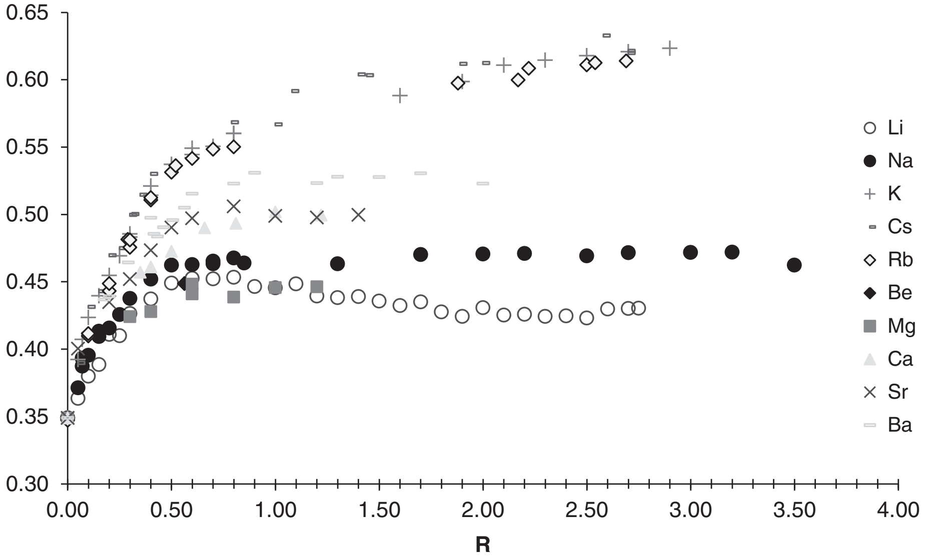

Figure 1.5. Packing fractions from a series of alkali and alkaline-earth borate glasses. R is the molar ratio of alkali oxide to boron oxide [8].

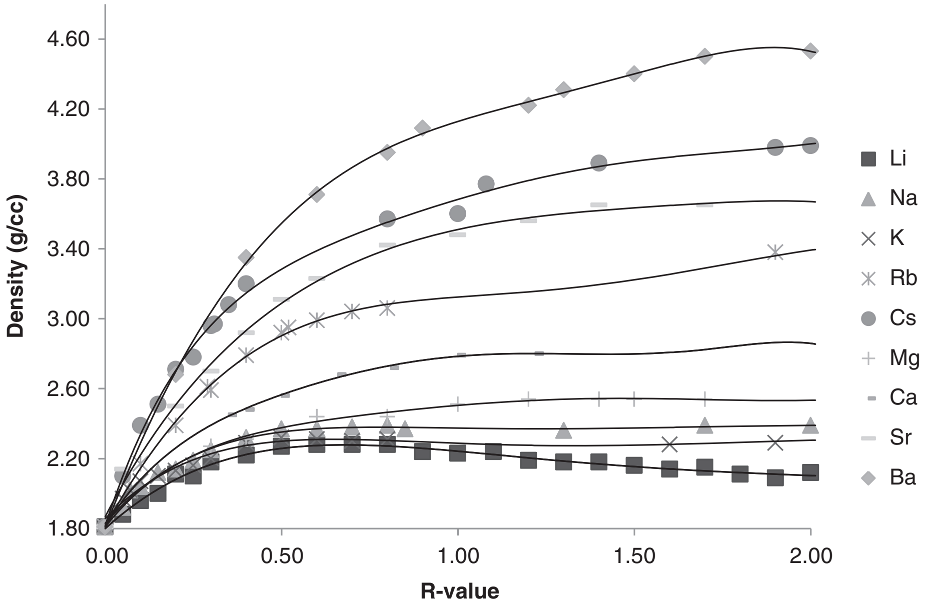

Figure 1.6. The density of alkali and alkaline-earth borates as a function of R, the molar ratio of modifying oxide to boron oxide [5]. The error is smaller than the symbols. See plate section for a color version of this figure.

TABLE 1.2. Volumes of the alkali borate short-range order groups [5].

System	Unit	Least squares derived volumes of the structural groups
Li	Q^{33}	0.98
	Q^{44}	0.94
	Q^{32}	1.28
	Q^{31}	1.61
Na	Q^{33}	0.95
	Q^{44}	1.24
	Q^{32}	1.58
	Q^{31}	2.12
K	Q^{33}	0.95
	Q^{44}	1.66
	Q^{32}	1.99
	Q^{31}	2.95
Rb	Q^{33}	0.98
	Q^{44}	1.92
	Q^{32}	2.27
	Q^{31}	3.41
Cs	Q^{33}	0.97
	Q^{44}	2.28
	Q^{32}	2.62
	Q^{31}	4.13

Note: The volumes are reported relative to the volume of the $BO_{1.5}$ unit in B_2O_3 glass. The units are reported as Q^{ni} where the integer n refers to the boron coordination and i denotes the number of bridging oxygens per boron.

The reader is referred to an extensive literature on this topic [5, 8, 9, 10].

In general one sees that the volumes are strong functions of the alkali. The Q^{33} units are independent of alkali and hence are of similar size in each system (the reported values are best-fit values for all compositions at which the unit is present). The other units show an expected increase with increasing non-bridging oxygen (NBO) content and increasing alkali content. In some cases involving potassium, rubidium, and cesium the volumes of the structural units are dominated by the alkali's ionic volume.

1.1.5 Case Studies from Some Glass Systems

1.1.5.1 Lithium Silicates Among the most basic glass systems are the lithium silicates. Figure 1.7 presents the densities of this system determined by Peters et al. [10] using the sink-float method as a function of J, the molar ratio of lithia to silica. The figure also depicts a literature compilation of densities from Bansal and Doremus [11].

The sink-float method agrees well with the literature compilation by Bansal and Doremus [10, 11] except that the scatter is larger since the error in this one study is one percent versus the compiled data of 16 independent studies, whose error is far less.

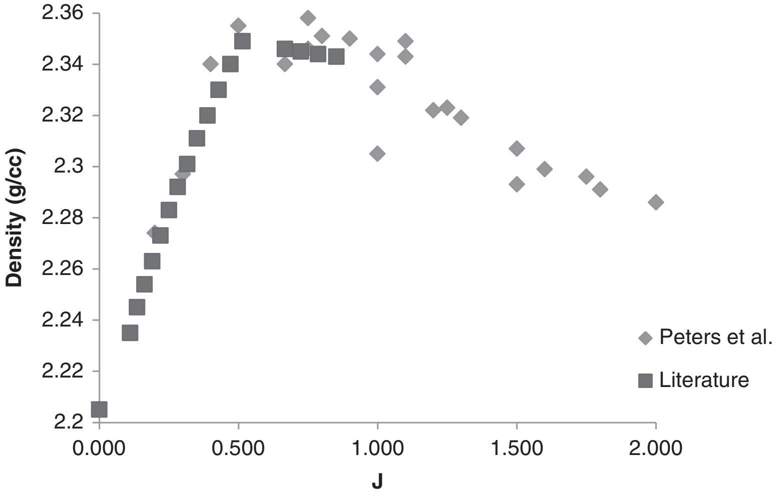

Figure 1.7. Density of lithium silicate glasses by the sink-float method from Peters et al. [10] and a comparison of literature values compiled by Bansal and Doremus [11]. J is the molar ratio of lithium oxide to silicon dioxide.

The changing atomic structures in this system are closely approximated by Q^i units shown in Figure 1.8.

The abundances of these units closely follow a simplified lever rule model [10] as shown below and in Figure 1.9:

$$Q^4 = 1 - 2J \quad Q^3 = 2J \quad 0.0 \le J \le 0.5 \tag{1.18a}$$

$$Q^3 = 2 - 2J \quad Q^2 = 2J - 1 \quad 0.5 \le J \le 1.0 \tag{1.18b}$$

$$Q^2 = 3 - 2J \quad Q^1 = 2J - 2 \quad 1.0 \le J \le 1.5 \tag{1.18c}$$

$$Q^1 = 4 - 2J \quad Q^0 = 2J - 3 \quad 1.5 \le J \le 2.0 \tag{1.18d}$$

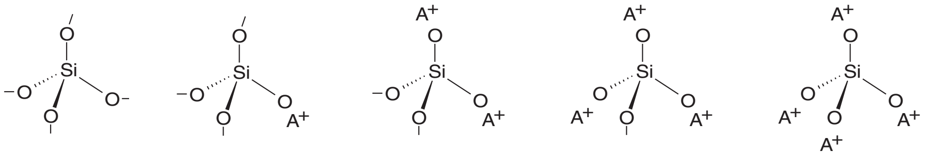

Figure 1.8. The Q^i structural units found in alkali silicate glasses, from left to right they advance from Q^4 to Q^0 where the superscript denotes the numbers of bridging oxygens per Si. A^+ represents an alkali ion.

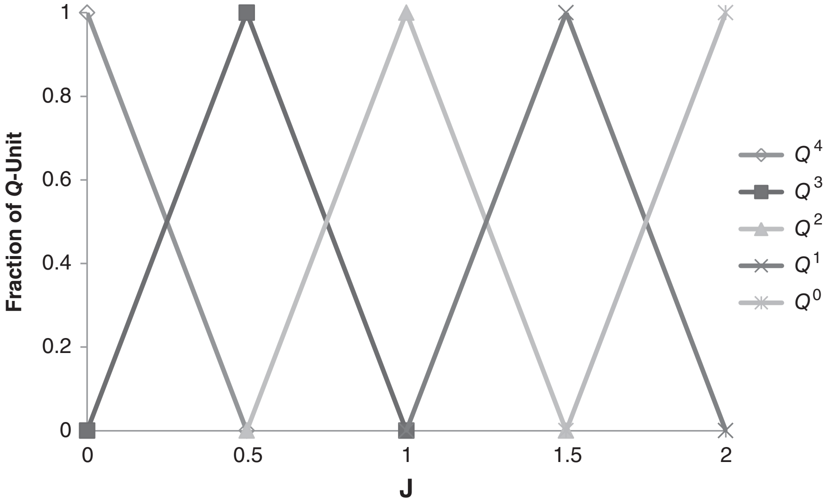

Figure 1.9. The lever rule for lithium silicate glasses.

Notice in Figure 1.7 the sharp transition in density near J = 0.5. This is the composition at which there is a significant structural rearrangement in the silicates as it is the Q^3 composition that lies at the boundary between Q^4 changing to Q^3 and the consequent compositional region where Q^3 adds an NBO to form Q^2 units. This may also be seen in the volume per mole silica as shown in Figure 1.10.

Note that using the volume per mole silica linearizes the molar volume results. This results in the slope of each linear region representing the volume change for the silicate structural units as follows:

$$Q^4 \rightarrow Q^3 \text{ for } J < 0.5 \text{ and} \tag{1.19a}$$

$$Q^3 \rightarrow Q^2 \text{ for } 0.5 < J < 1.0 \tag{1.19b}$$

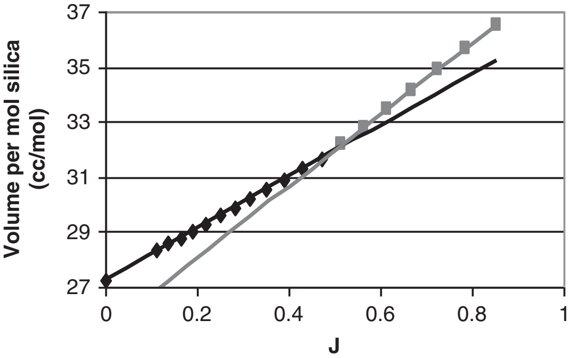

Figure 1.10. Volume per mol silica from a series of lithium silicate glasses, $JLi_2O.SiO_2$. The data are taken from Bansal and Doremus [11]. J is the molar ratio of lithium oxide to silica.

TABLE 1.3. Relative volumes of the silicate units in $Li_2O.SiO_2$ glasses. All volumes are relative to the volume of the SiO_2 tetrahedron in silica glass.

Unit	Least squares derived volumes of the structural groups
Q^4	1.00
Q^3	1.17
Q^2	1.41
Q^1	1.69
Q^0	1.95

Equations 1.18 (a–d) and the density may be linked together to find the volumes of the lithium silicate structural groups by insertion in Eq. 1.17 and the use of a least squares analysis. This yields the volumes given in Table 1.3[10].

1.1.5.2 Alkali Borates Shown in Figure 1.11 is the density of the lithium borate glass system as a function of R, the molar ratio of lithia to bora. These data are from the paper by Shibata et al. [12]. Also shown in the figure is the tetrahedral fraction of borons, f_2, as found in Jellison, Feller, and Bray's 1978 paper [13]. The two quantities track each other well indicating a strong connection between atomic arrangement and physical property.

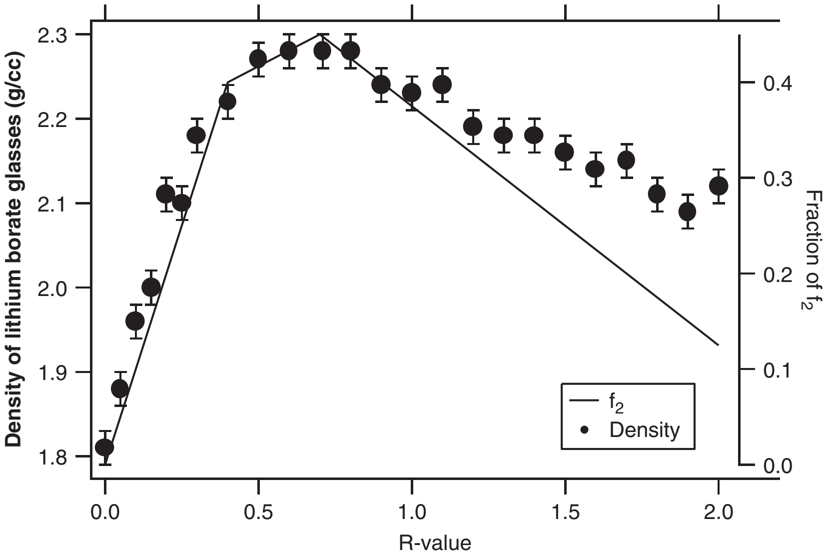

Figure 1.11. Density of lithium borate glasses as a function of R, the molar ratio of lithium oxide to boron oxide [12]. Also shown in the figure is the fraction, f_2, of tetrahedral borons [13].

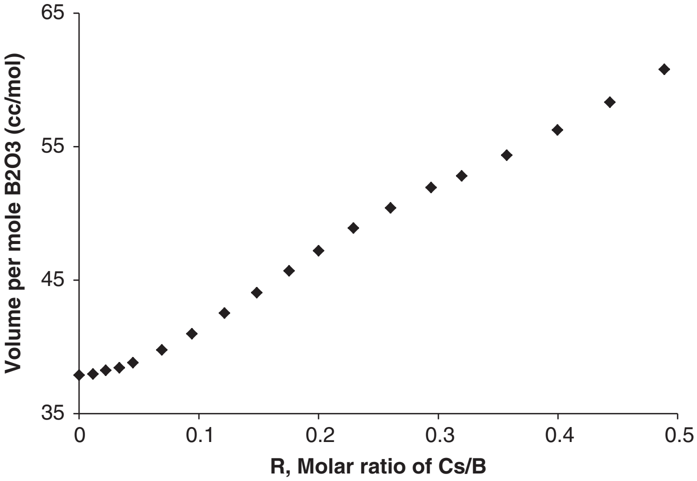

Figure 1.12. Volumes per mole B_2O_3 of the cesium borate glass system from Kodama [3] The error is less than the symbol size.

Shown in Figure 1.12 are the precise density data of Kodama [3] from the cesium borate system. These data, presented as the volume per mole boron oxide, from very homogeneous glasses prepared for velocity of sound measurements are accurate to better than 0.1 %. The undulations appearing in the density trend are real and represent subtle density fluctuations that have been correlated to intermediate range structures such as triborate and diborate rings [3], see Figure 1.13.

A further example of the utility of density data is found in a comparison of elastic properties with molar volumes. Using Kodama's density data, the molar volumes of the alkali borates are shown in Figure 1.14. The reader may see further evidence for intermediate range order in the systematic variations of the molar volume as alkali content, R, increases.

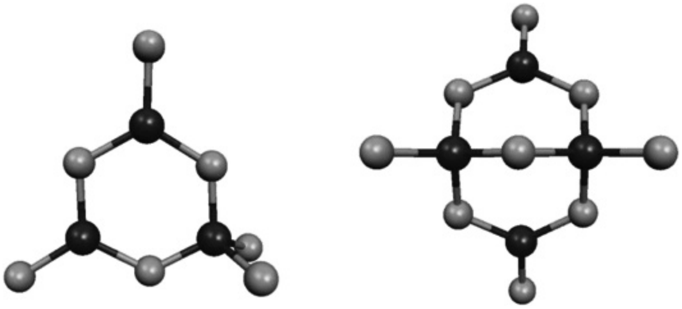

Figure 1.13. The triborate and diborate superstructural groups.

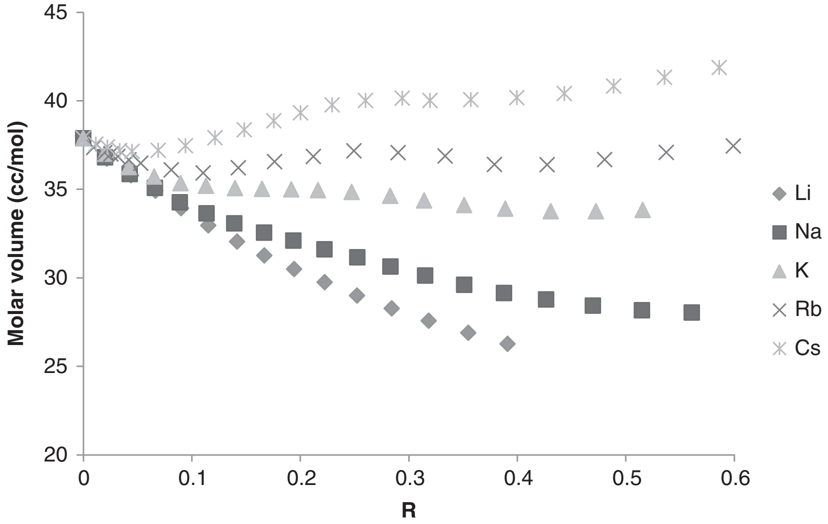

Figure 1.14. Molar volumes of the alkali borates using Kodama's data as a function of R, the molar ratio of alkali oxide to boron oxide [3].

Kodama also found the elastic constants for the system using velocity of sound measurements. A representative example, stiffness, is shown below in Figure 1.15 as R is changed [3].

Next, we examine the stiffness as a function of molar volumes for the representative cesium borate case [3], see Figure 1.16.

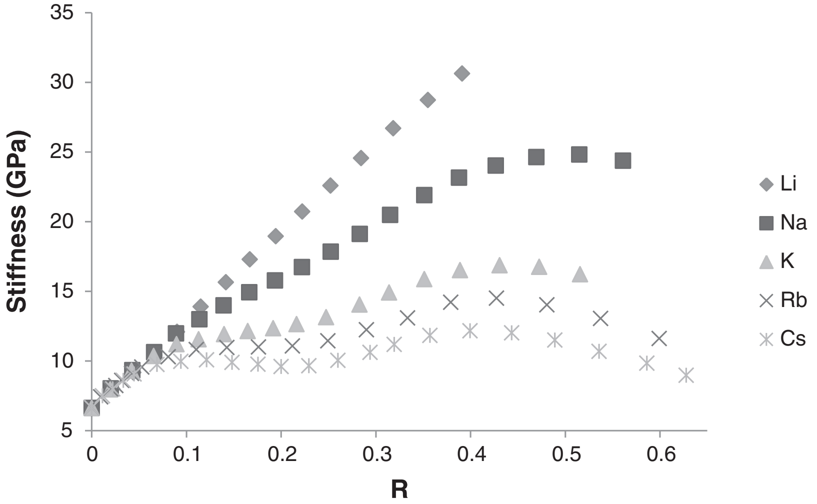

Figure 1.15. Stiffness as a function of composition, R [3].

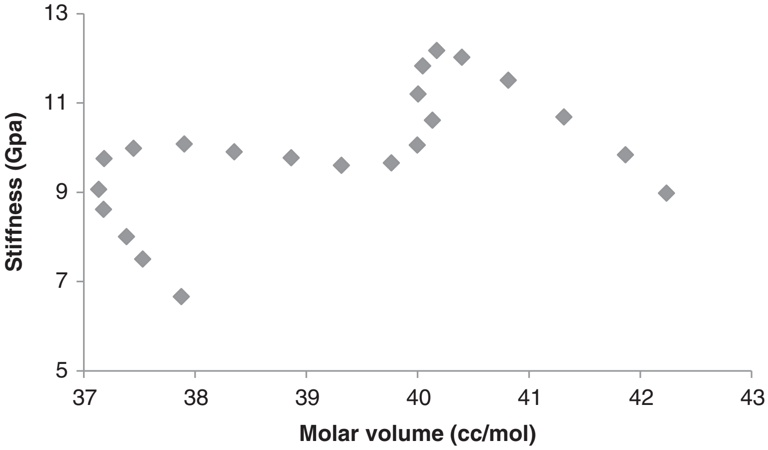

Figure 1.16. Stiffness as a function of molar volumes for the cesium borate case [3].

The trend of stiffness versus molar volume maybe understood in terms of simultaneous volume and stiffness changes [3]. The values for B_2O_3 may be found in the lower left part of the figure (molar volume just under 38 cc/mol and stiffness of just under 7 GPa). From there the amount of cesium modifier increases as one traces the data first to lower molar volumes then to higher ones. Initially, the glass shrinks as tetrahedral borons form; this results in a stiffer glass as the stiffness surpasses 9 GPa. Then the glass expands as the stiffness remains approximately constant. This maybe attributed to the formation of open triborate rings. Then, near 40 cc/mol, the glass ceases to expand but stiffens instead; this behavior is likely due to the formation of tight and compact diborate groups. Further addition of cesium oxide causes the formation of non-bridging oxygens on the borons, destroying the superstructural groups and opening up the structure. The molar volume increases as the glass becomes less stiff.

1.1.6 Conclusion to Density Measurements

Density is of fundamental importance in glass physics. It is measured using a wide variety of techniques depending on the sample and the desired precision.

Knowledge of the density is crucial in the various scattering experiments employing x-rays, electrons, and neutrons. Also, any structural model for atomic arrangements must pass the density test: does the model predict the correct density?

Density is used to determine a variety of volumes such as molar volume, volume per mole glass former, and atomic level structural volumes. Furthermore, density is used to determine packing fractions that, in effect, represent density in a dimensionless way.

Part III: Thermal Effects with a Focus on the Glass Transition Temperature

1.2 OVERVIEW

In this part of the chapter we will go through how thermal events and particularly the glass transition temperature, T_g, are determined in a number of ways. As with density it is impossible to uniquely go from experimental T_gs to the true representation of atomic arrangements. T_g is affected by many factors but the principal one of interest in this chapter will be atomic arrangements in a manner analogous to the density discussed in Part II of this chapter. T_g data have become available from a wide variety of glass systems over extended compositional regimes [14]. Hence, it has become possible to gain greater insights into atomic arrangement variations between systems. As stated before, what has emerged from this work is a comprehensive set of data which has been linked to models of the short and intermediate range order.

1.3 EXPERIMENTAL METHODS AND THEORY

1.3.1 Calorimetry

1.3.1.1 Differential Scanning Calorimetry A differential scanning calorimeter (DSC) is composed of two matched electrical heating elements that are programmed to simultaneously heat two sample holders with encapsulated pans in them. This occurs in such a way as to raise the temperature of both pans at the same heating rate [15]. A well-known method to accomplish this is to “power compensate” for the presence of a sample in a pan (usually aluminum) on one side and a blank pan on the other. The result of the experiment is a thermogram as shown in Figure 1.17. The vertical scale is given in differential power, typically in mW. In this figure, vertically downward displays endothermic events in which heat enters the system. whereas vertically upward shows exothermic reactions in which heat leaves the system.

This figure has three typical thermodynamic reactions shown in it. Going from low to high temperatures one can first see a *change in specific heat* (measured by an increased endothermic differential power level) as is typically seen in a glass transition. The *exothermic event* involves the removal of energy from the sample compared to the blank reference pan. A representative exothermic reaction is the crystallization event. Thus, a glass that crystallizes upon heating enters a more ordered state and heat must be released from the sample for this to happen. The final endothermic event is due to the melting of the crystalline phase.

Each of these events has assigned temperatures. The temperature for the onset of the glass transition, where the steepest part of the change in the specific heat part of the thermogram curve meets the pre-event baseline is known as the onset T_g. In similar fashion $T_{\mathrm{m\,onset}}$ (or $\mathrm{T_s}$) for melting maybe determined. The onset end of melting is known as $T_{\mathrm{m\,endpoint}}$, whereas the temperature marking the crystallization is defined in

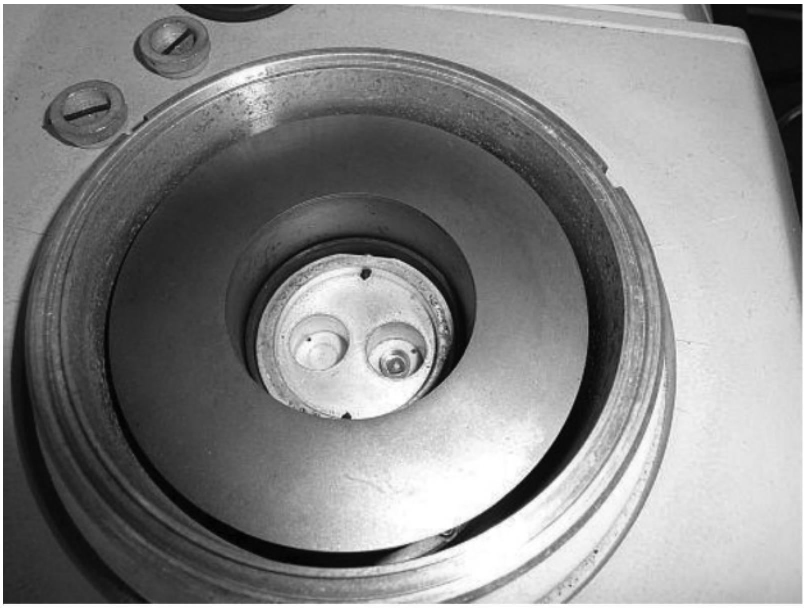

Figure 1.17. The DSC head uncovered for sample insertion (from Wikipedia).

the same onset way is known as the T_x (onset) or $T_x{}^h$ whereas T_C is the temperature at the thermogram exothermic minimum for the crystallization event).

Please note that the thermal events are referenced to a baseline, typically run just before the sample run. A baseline is run with no sample in either pan and the expected

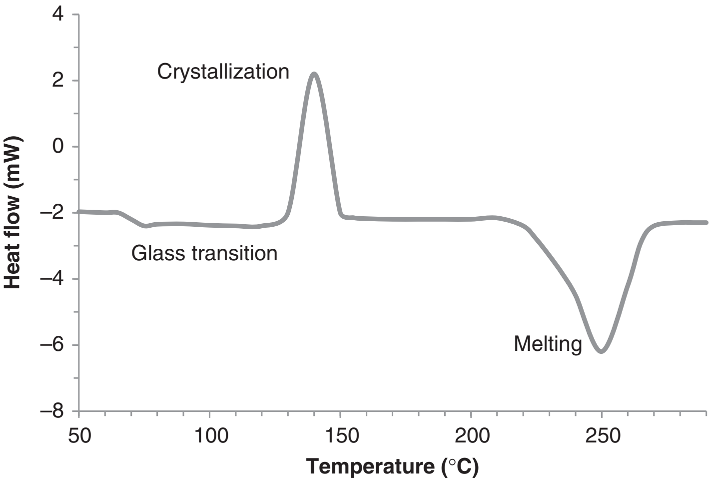

Figure 1.18. Representative thermogram from a DSC

result is a flat signal. In the usual real case, the baseline will have some small deviation from being entirely flat and software maybe used to both correct and subtract the baseline from an experimental run in order to normalize it to a flat baseline.

Calibration occurs by using materials with known melting points, typically metals such as indium, lead, and zinc.

1.3.1.2 Some Practical Considerations of DSC Care must be taken to maintain the heating elements in good working order by routinely cleaning the sample cup areas. The modern DSC comes with software designed to run the temperature up and down in a cleaning cycle. Usually the heating elements are so well matched that damage to one side necessitates full replacement of the head where the heating elements reside. This is a fairly expensive repair at the level of thousands of US dollars.

The sample pans may be made of a variety of materials including aluminum (good up to 600°C), gold (useful up to 1000°C), platinum (may be used to near 1700°C), or ceramic (useful to a variety of temperatures). Usually the aluminum pans are discarded after single use. These aluminum pans typically cost a few dollars each.

1.3.1.3 Modulated DSC This is a patented technique of the TA Instruments and to some extent reworked by other companies. To quote TA [16],

> *MDSC offers all the benefits of standard DSC, overcomes its limitations, and provides further information for greater understanding of material properties. Specifically, MDSC permits separation of the total heat flow signal into its thermodynamic (heat capacity) and kinetic components. MDSC offers simultaneous improvements in sensitivity and resolution, and can separate overlapping events that are difficult or impossible to do by standard DSC.*

This is a manifold topic and details beyond the introduction presented here are available from either vendors or more specialized works.

1.3.2 Differential Thermal Analysis

Differential thermal analysis (DTA) is a closely related technique to differential scanning calorimetry. In it a furnace heats two samples. One is a reference sample of alumina and the other a mixture of alumina and the glass in question. Each sample has its temperature measured by a thermocouple and the difference in temperature between the two thermocouples is plotted versus temperature of the sample as the furnace is ramped up in temperature. The plot may be converted to power difference as a function of sample temperature as in the DSC or directly plotted as temperature difference versus temperature of the sample, see Figure 1.19. The thermal events described for DSC show up in analogous manner in DTA.

Its chief advantage over DSC is its relatively inexpensive way to reach high temperatures. On the other hand the rate of temperature change is harder to control due to the rather large thermal mass associated with the furnace.

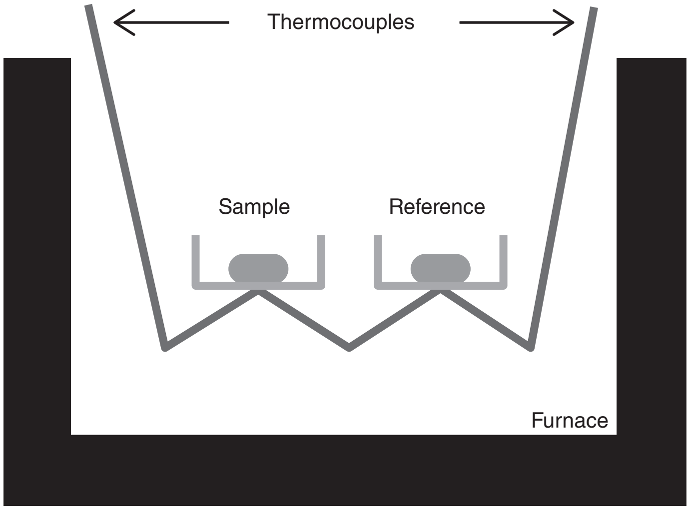

Figure 1.19. A schematic of the operation of a DTA.

Like in the DSC, calibration occurs by using materials with known melting points, typically metals.

1.4 INSTRUMENTATION USED FOR DETERMINING T_g AND RELATED THERMAL EVENTS

1.4.1 DSCs

DSCs are sold commercially and come in several varieties. Shown in Figure 1.20 is a current TA® Modulated DSC. Typical temperature calibration accuracy is better than +/− 0.1°C whereas the error in T_g is close to +/− 3.0°C.

DSCs need some accessories. These include sample pans, crimpers, cover lid reformers, standard metals for calibration, and more.

1.4.2 Differential Thermal Analysis

Many commercial versions of DTAs are available, see Figure 1.21. They consist of a furnace and typically two ceramic stalks on which the samples reside along with a thermocouple for each. Typical temperature calibration accuracy is better than +/− 0.1°C whereas the error in T_g, T_x, or T_m, is of the order of +/− 1.0 to 3.0°C.

It is also possible to purchase simultaneous thermal analysis (STA) instruments. In such instruments, there are simultaneous DTA and thermogravimetric analysis (TGA) measurements that take place.

Figure 1.20. A TA® modulated DSC.

Figure 1.21. A Netzsch® DTA.

Similar accessories to the DSC are needed in DTA. Usually ceramic sample cups are used and aluminum oxide is coplaced with the sample in the ceramic sample cup.

1.5 ANALYSIS OF DATA AND EXTRACTION OF USEFUL INFORMATION

Figure 1.22 shows an experimental thermogram [17] from a lithium borate glass with composition $1.5Li_2O.B_2O_3$. The thermal run was carried out at 10°C/min in a 404 Netzsch DSC. It has several clearly delineated thermal events as marked (all in °C):

R, Li/B ratio	Mole % Li_2O	T_g	T_x	T_c	$T_{\text{m onset}}$	$T_{\text{m endpoint}}$
1.5	60.0	315	369	382	692	790

These temperatures are determined as shown in the figure. Proprietary software was used to determine onset or other values of the required temperatures.

The *fictive temperature* is defined as the temperature at which the melt that formed the glass was at as the sample solidified may also be found from DSC. This is beyond the present discussion.

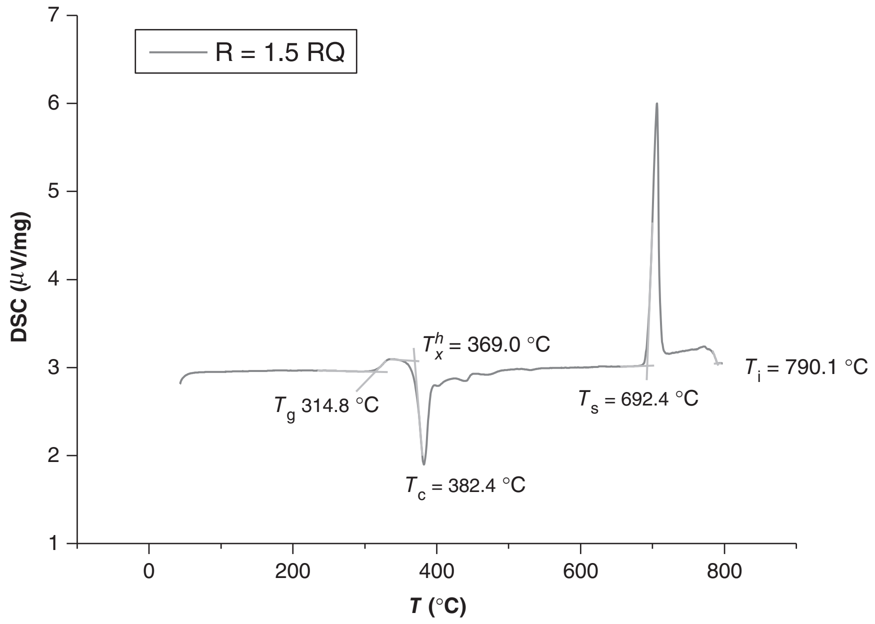

Figure 1.22. A Typical DSC thermogram [17]. It is from a lithium borate glass with R = 1.5, where R is the molar ratio of alkali oxide to boron oxide. Note that endothermic/exothermic directions are reversed from what was given earlier in the chapter.

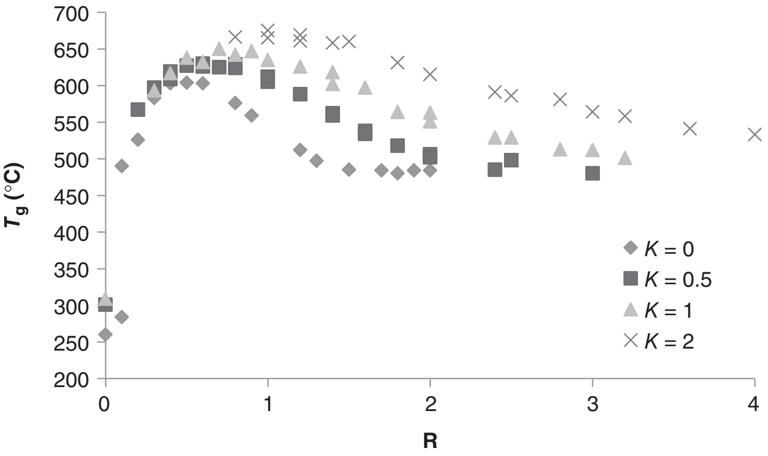

Figure 1.23. The T_gs of barium borosilicate glasses of the form $RBaO.B_2O_3.KSiO_2$ [18].

1.6 CASE STUDIES FROM GLASS SYSTEMS

1.6.1 The Glass Transition Temperatures of Barium Borosilicate Glasses [18]

The T_gs of a large series of barium borosilicate glasses of the form $RBaO.B_2O_3.KSiO_2$ were determined. The results are shown as families of K, with R varying widely as shown in Figure 1.23. The next illustration, Figure 1.24, depicts N_4, the fraction of four

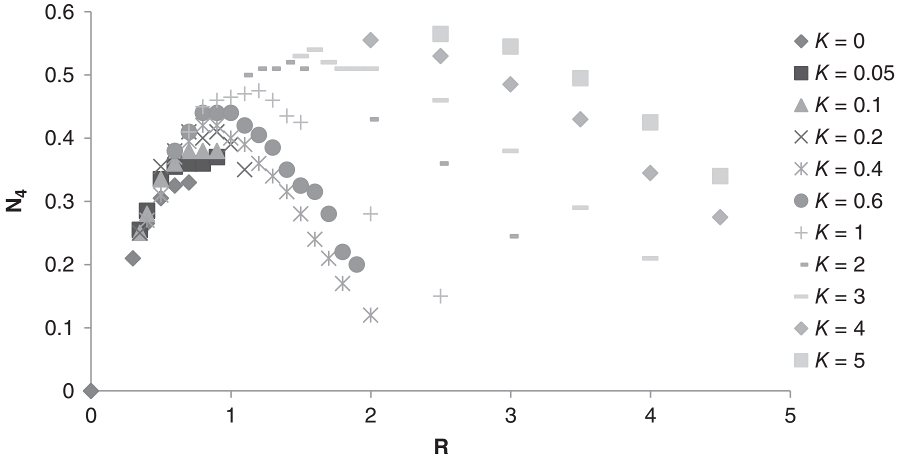

Figure 1.24. The fraction of four-coordinated borons, N_4, of barium borosilicate glasses of the form $RBaO.B_2O_3.KSiO_2$ [19].

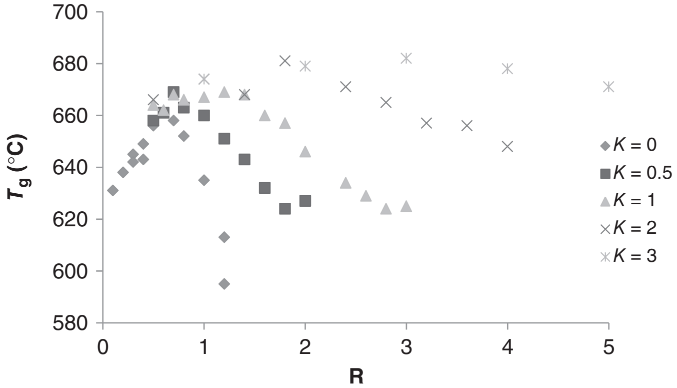

Figure 1.25. The T_gs of calcium borosilicate glasses of the form $RCaO.B_2O_3.KSiO_2$ [18].

coordinated borons present in these glasses as a function of R for fixed K families as well [19]. The following trends are observed.

- All T_g trends from various K families resemble the K = 0 family except the trends are shifted towards higher R as K increases. This is indicative of the sharing of alkali between the borate and silicate network with the borate network determining the T_g trend.
- The T_g maximum increases as K increases. This increase of the T_g maximum is attributed to the formation of a Si-O-B network. In contrast, Figure 1.25 shows this feature is not strongly present in calcium borosilicate glasses, implying the absence of strong network–network interactions.
- The T_g trends resemble closely the trends for N_4. However, unlike in the lithium borosilicate case [20], Figure 1.26, the T_gs remain high as R increases. This is likely due to crosslinking of Ba to two oxygens in the network. The same effect resulting in enhanced T_g values is present in the calcium borosilicate system as shown in Figure 1.25.

1.6.2 Stability Parameters in Lithium Borate Glasses [18]

Lithium borate glasses make a particularly good system to study thermal stability because of their relatively wide glass formation range, through the use of roller quenching. For glasses written $RLi_2O.B_2O_3$, this continuous range is from R = 0 to 2.8 (0 to 74 molar percent Li_2O) [12].

Table 1.4 depicts various literature definitions of stability parameters. Once the thermograms of the lithium borate glasses were measured and analyzed the following results were obtained as shown in Table 1.5 [18].

Most of the parameters for stability work reasonably well as guides for relative glass stability. In Figures 1.27a, 1.27b, 1.28a, and 1.28b are some representative stability

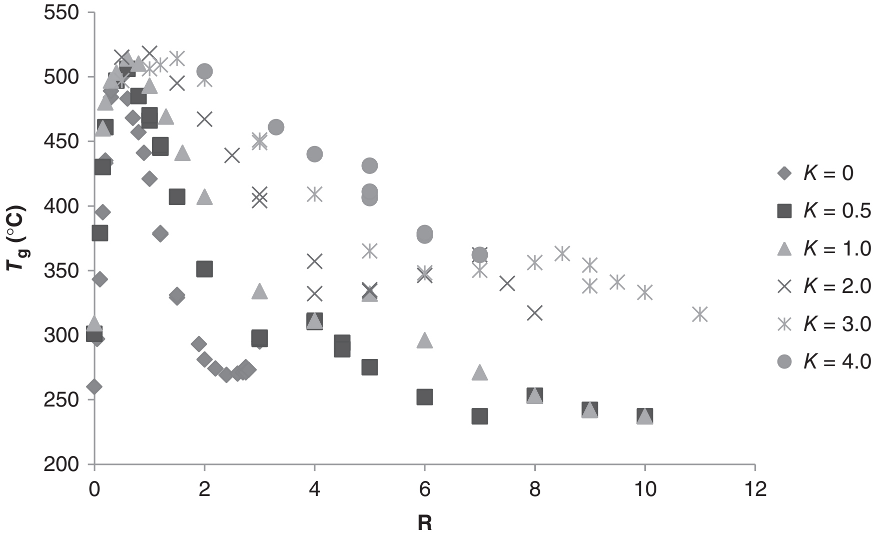

Figure 1.26. The T_gs of lithium borosilicate glasses of the form $RLiO.B_2O_3.KSiO_2$ [20]. See plate section for a color version of this figure.

TABLE 1.4. Glass stability parameters (temperatures in K) [17].

$$K_{LL} = \frac{T_x^h}{T_g + T_m}$$

$$K_H = \frac{T_x^h - T_g}{T_m - T_x^h}$$

$$K_W = \frac{T_x^h - T_g}{T_m}$$

$$K_T = \frac{T_g}{T_m}$$

$$K_{SP} = \frac{\left(T_x^h - T_g\right)\left(T_c^h - T_x^h\right)}{T_g}$$

$$K_1 = T_m - T_g$$

$$K_2 = T_x^h - T_g$$

$$K_3 = \frac{T_x^h}{T_m}$$

$$K_4 = \frac{\left(T_x^h - T_g\right)\left(T_c^h - T_x^h\right)}{T_m}$$

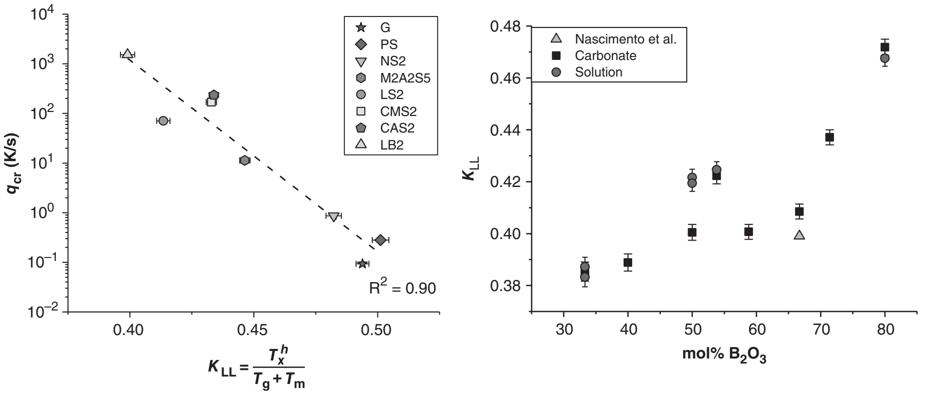

(a) (b)

Figure 1.27. (a), Critical cooling rate versus the glass stability parameter K_{LL} for several glasses [GeO2 (G), PbO.SiO2 (PS),Na2O.2SiO2 (NS2), 2MgO.2Al2O3.5SiO2 (M2A2S5), Li2O.2SiO2 (LS2), CaO.MgO.2SiO2 (CMS2),CaO.Al2O3.2SiO2 (CAS2), Li2O.2B2O3 (LB2)]. (b), the same K_{LL} versus composition in the $Li_2O–B_2O_3$ system [17].

results to show how careful DSC experiments maybe used to track critical cooling rates. Note that in each figure there is a presentation of a calibration curve found from glasses in the literature that confirm the connection between critical cooling rates and the stability parameter. Thus, it is possible to determine close values for the critical cooling rates of lithium borate glasses.

The glasses with low borate content have stability parameters that are readily translated to critical cooling rates using the calibration curves in Figures 1.27 and 1.28,

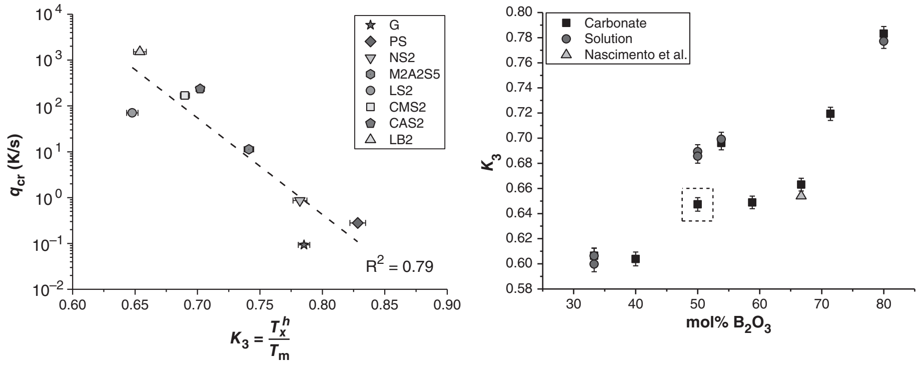

(a) (b)

Figure 1.28. (a), Critical cooling rate versus the glass stability parameter K_3 for several glasses [GeO2 (G), PbO.SiO2 (PS),Na2O.2SiO2 (NS2), 2MgO.2Al2O3.5SiO2 (M2A2S5), Li2O.2SiO2 (LS2), CaO.MgO.2SiO2 (CMS2),CaO.Al2O3.2SiO2 (CAS2), Li2O.2B2O3 (LB2)]. (b), Glass stability parameter $K_3 = T_x^h/T_m$ versus composition [17].

TABLE 1.5. Characteristic temperatures (°C) from lithium borate glasses.

R	Mole % Li_2O	Method*	T_g	T_x	T_c	T_s	$T_{m\ onset}$	$T_{m\ endpoint}$
0.25	20.0	Carbonate method	460	597	622	726	–	837
		Solution method	461	588	614	770	–	835
0.4	28.6	Carbonate method	489	576	585	722	–	907
			489	583	591	716	–	–
0.5	33.3	Carbonate method	463	510	516	806	908	926
0.7	41.2	Carbonate method	459	494	511	636	820	909
0.86	46.2	Carbonate method	439	491	500	–	825	846
		Solution method	436	494	500	–	823	844
1.0	50.0	Carbonate method	411	445	452	–	836	856
		Solution method	420	480	488	–	819	850
		Solution method II	420	475	483	–	818	850
1.5	60.0	Carbonate method	315	369	382	–	692	790
2.0	66.7	Solution method	265	298	300	596	643	679
		Solution method II	272	311	313	595	630	690
		Carbonate method	272	303	306	–	629	677

Estimated error in temperatures is approximately ± 3–5°C.

*Glasses were prepared in two ways, from lithium carbonates and boric acid heated using a traditional furnace approach and by a solution route to glass formation using lithium hydroxide and boric acid solutions.

See Table 1.5. The resulting critical cooling rates approach 10^4 to 10^5 K/s—exactly what was needed to make these glasses using roller quenching.

1.7 CONCLUSION TO THERMAL PROPERTIES

Using modern instrumentation, a large variety of thermal measurements are possible. These include characteristic temperatures associated with the glass transition, crystallization, melting, and more. These measurements maybe compared with models for atomic arrangement. Critical cooling rates for glass formation may be deduced by suitable combinations of the thermal parameters.

Oftentimes, thermal properties provide a mirror to atomic-level or intermediate range structure.

The T_g itself is an important intrinsic value when choosing reliable and stable glasses for practical commercial purposes.

ACKNOWLEDGMENTS

The National Science Foundation is thanked for support under grant number NSF-DMR-0904615.

Ethan Lawrence is thanked for help with the figures.

REFERENCES

References on Density

1. M. Shibata, C. Sanchez, H. Patel, J. Stark, S. Feller, G. Sumcad, and J. Kasper, *J. Non-Cryst. Solids* **85**, 29–41 (1986).
2. S. Giri, C. Gaebler, J. Helmus, M. Kodama, M. Affatigato, and S. Feller, *J. Non-Cryst. Solids* **347**, 87–92 (2004).
3. S. Feller, M. Affatigato, S. Giri, A. Basu, and M. Kodama, *Phys. Chem. Glasses* **44**(2), 117–120 (2003).
4. H.C. Lim and S. Feller, *Diffus. Defect Data* **53-54**, 277–282 (1987).
5. N.P. Lower, J.L. McRae, H.A. Feller, A.R. Betzen, S. Kapoor, M. Affatigato, and S.A. Feller, *J. Non-Cryst. Solids* **293-295**, 669–675 (2001).
6. S. Feller, N. Lower, and M. Affatigato, *Phys. Chem. Glasses* **42**(3), 240–246 (2001).
7. R.D. Shannon, *Acta. Crystallogr.* **A 32**, 751 (1976).
8. M. Burgess, D. McClarnon, M. Affatigato, and S. Feller, *J. Non-Cryst. Solids* **354**, 3491–3502 (2008).
9. B.C.L. Chong, S.H. Choo, S. Feller, B. Teoh, O. Matthews, E.J. Khaw, D. Feil, K.H. Chong, M. Affatigato, D. Bain, K. Hazen, K. Farooqui, *J.Non-Cryst.Solids* **109**, 105–113 (1989).
10. A.M. Peters, F.M. Alamgir, S.W. Messer, S. Feller, and K.L. Loh, *Phys. Chem. Glasses* **35**(5), 212–215 (1994).
11. N. Bansal and R. Doremus, *Handbook of Glass Properties*, Academic Press, Orlando, 1986.
12. M. Shibata, C. Sanchez, H. Patel, J. Stark, S. Feller, G. Sumcad, and J. Kasper, *J. Non-Cryst. Solids* **85**, 29–41 (1986).
13. G.E. Jellison, Jr., S. Feller, and P.J. Bray, *Phys. Chem. Glasses* **19**, 52–53 (1978).

References on Thermal Properties

14. See the *SciGlass Database*, for example.
15. D.A. Skoog, F.J. Holler, and S.R. Crouch, *Principles of Instrumental Analysis* (6th Edition), Thomson: Belmont, CA, 2007, pp. 900–901.
16. http://www.tainstruments.com/main.aspx?siteid=11&id=86&n=6
17. E.B. Ferreira, E. Zanotto, S.A. Feller, G. Lodden, J. Banerjee, T. Edwards, and M. Affatigato, *J. Am. Chem. Soc.* **94** (11), 3833–3841 (2011).
18. S. Feller, T. Mullenbach, M. Franke, S. Bista, A. O'Donovan-Zavada, K. Hopkins, D. Starkenberg, J.McCoy, D. Leipply, J. Stansberry, M. Affatigato, D. Holland, M. Smith, S. Kroeker, V. Michaelis, and J. Wren, *Phys. Chem. Glasses Eur. J. Glass Sci. B* **53** (5), 210–218 (2012).
19. Stallworth, P. E. Ph.D. Thesis, Brown University (1989).
20. R. Boekenhauer, H. Zhang, D. Bain, S. Feller, S. Kambeyanda, K. Budhwani, and P. Pandikuthira, *J. Non-Cryst. Solids* **175**, 137–144 (1994).